In vivo imaging of Aminopeptidase N (CD13) receptors in experimental renal tumors using the novel radiotracer ^{68}Ga-NOTA-c(NGR)

Gábor Máté[a], István Kertész[a], Kata Nóra Enyedi[b], Gábor Mező[b], János Angyal[c], Nikolett Vasas[d], Adrienn Kis[a], Éva Szabó[c], Miklós Emri[a], Tamás Bíró[d], László Galuska[a,1], György Trencsényi[a,e,1,*]

[a]Department of Nuclear Medicine, University of Debrecen, Hungary, [b]MTA-ELTE, Research Group of Peptide Chemistry, Hungarian Academy of Sciences, Eötvös L. University, Budapest, Hungary, [c]Department of Periodontology, [d]Department of Physiology, University of Debrecen, Debrecen, Hungary, [e]Scanomed LTD, Debrecen, Hungary

Keywords: ^{68}Ga-NOTA-c(NGR); ^{68}Ga-NODAGA-[c(RGD)]$_2$; Aminopeptidase N (CD13) expression; Renal tumors; Tumor angiogenesis; Positron Emission Tomography

[1]These authors contributed equally to this study.

[*] To whom correspondence may be addressed. P.O.B. 63 Debrecen, Nagyerdei krt. 98.
E-mail: trencsenyi.gyorgy@med.unideb.hu

Abstract

Purpose: Aminopeptidase N (APN/CD13) plays an important role in tumor neoangiogenic process and the development of metastases. Furthermore, it may serve as a potential target for cancer diagnosis and therapy. Previous studies have already shown that asparagine-glycine-arginine (NGR) peptides specifically bind to APN/CD13. The aim of the study was to synthesize and investigate the APN/CD13 specificity of a novel ^{68}Ga-labeled NOTA-c(NGR) molecule *in vivo* using miniPET.

Methods: c[KNGRE]-NH_2 peptide was conjugated with *p*-SCN-Bn-NOTA and was labeled with Ga-68 (^{68}Ga-NOTA-c(NGR)). Orthotopic and heterotopic transplanted mesoblastic nephroma (NeDe) bearing Fischer-344 rats were prepared, on which biodistribution studies and miniPET scans were performed for both ^{68}Ga-NOTA-c(NGR) and $\alpha_v\beta_3$ integrin selective ^{68}Ga-NODAGA-$[c(RGD)]_2$ tracers. APN/CD13 receptor expression of NeDe tumors and metastases was analyzed by western blot.

Results: ^{68}Ga-NOTA-c(NGR) was produced with high specific activity (5.13-5.92 GBq/μmol) and with excellent radiochemical purity (95%<), at all cases. Biodistribution studies in normal rats showed that uptake of the ^{68}Ga-NOTA-c(NGR) was significantly ($p \leq 0.05$) lower in abdominal organs in comparison with ^{68}Ga-NODAGA-$[c(RGD)]_2$. Both radiotracers were mainly excreted from the kidney. In NeDe tumor bearing rats higher ^{68}Ga-NOTA-c(NGR) accumulation was found in the tumors than that of the ^{68}Ga-NODAGA-$[c(RGD)]_2$. Using orthotopic transplantation, metastases were developed which showed specific ^{68}Ga-NOTA-c(NGR) uptake. Western blot analysis confirmed the presence of APN/CD13 expression in NeDe tumors and metastases.

Conclusion: Our novel radiotracer ^{68}Ga-NOTA-c(NGR) showed specific binding to the APN/CD13 expressed ortho- and heterotopic transplanted NeDe tumors. Therefore, ^{68}Ga-NOTA-c(NGR) is a suitable tracer for the detection of APN/CD13 positive tumors and metastases *in vivo*.

Abbreviations

APN	aminopeptidase N
Boc	*terc*-butyloxycarbonyl
BOP	(benzotriazol-1-yloxy)tris(dimethylamino)phosphonium hexafluorophosphate
ClZ	2-chlorobenzyloxycarbonyl
CBCT	cone-beam computer tomography
c(KNGRE)-NH_2	cyclic(lysine-asparagine-glycine-arginine-glutamic acid amide)
DIEA	*N*-diisopropylethylamine
DMF	dimethylformamide
DOTA	1,4,7,10-tetraazacyclododecane-1,4,7,10-tetraacetic acid
Fmoc	9-fluorenylmethoxycarbonyl
HOBt	1-hydroxybenzotriazole
i.p.	intraperitoneal
MeCN	acetonitrile
NGR	asparaginyl-glycyl-arginine
NODAGA	1,4,7-triazacyclononane-1-glutaric acid-4,7-acetic acid
NOTA	1,4,7-triazacyclononane-1,4,7-triacetic acid
RGD	argininyl-glycinyl-aspartic acid
PET	positron emission tomography
RCP	radiochemical purity
SRCA	subrenal capsule assay
TFA	triflouroacetic acid
TIS	triisopropylsilane
s.c.	subcutaneous

Chemical compounds studied in this article:

L-Arginine	CID: 6322
L-Asparagine	CID: 6267
(benzotriazol-1-yloxy)tris(dimethylamino) phosphonium hexafluorophosphate	CID 151348
N-diisopropylethylamine (DIEA)	CID 81531
dimethylformamide (DMF)	CID 6228
L-Glutamic acid	CID: 33032
Glyicine	CID: 750
1-hydroxybenzotriazole (HOBt)	CID 2796029
L-Lysine	CID: 5962
1,4,7-triazacyclononane-1,4,7-triacetic acid (NOTA)	CID 3036142
triflouroacetic acid (TFA)	CID 6422
triisopropylsilane (TIS)	CID 6327611

1. Introduction

Angiogenesis, the formation of new blood vessels from pre-existing vasculature is a fundamental physiological process (Simons 2005); nevertheless this process might be triggered and enhanced by many human diseases including cancer (Folkman 2002), congestive heart failure (Higuchi et al., 2008) , atherosclerotic plaque and peripheral artery disease (Carmeliet and Jain 2000; Wu et al., 2013). Numerous studies also suggest that tumor-vasculature formation is followed by a characteristic sequence of events, mediated and controlled by growth factors, adhesion molecules, and cellular receptors (Ellis et al., 2001; Yancopoulos et al., 2000), which can serve as a biochemical platform for targeted tumor diagnosis and therapy (Haubner et al., 1999, 2001; Wang et al., 2011; Dijkgraaf et al., 2013).
Related to this process, two important targets have already been revealed on the new tumor vasculatures; integrins (Ellis et al., 2001; Seong Choe et al., 2007; Haubner, 2006) and Aminopeptidase N (APN or CD13) (Pasqualini et al., 2000; Corti et al., 2008). The latter is a zinc-dependent, trans-membrane exopeptidase that also plays an important role in metastatic tumor cell invasion through enzyme-catalyzed degradation of extracellular matrix components (Rundhaug 2005). Furthermore, high expression of CD13 can be detected in a number of human solid tumors, including melanoma (van Hensbergen et al., 2004), prostate, lung and ovarian cancer (Chen et al., 2013).
An asparaginyl-glycinyl-arginine (NGR) sequence containing peptides have been identified *via* phage display as specific ligands of CD13 (Corti et al., 2008). Also, it was found to bear a threefold higher efficacy for the detection of neoangiogenic vessels than RGD (argininyl-glycinyl-aspartic acid) peptides (Buehler et al., 2006) that are widely used for the detection of $\alpha_v\beta_3$ and $\alpha_v\beta_5$ integrin-expression. As such, several studies have reported that the conjugation of an NGR motif with chemotherapeutic drugs might lead to improved and more specific tumor-therapy (Arap et al., 1998; Corti and Curnis 2011; Corti et al., 2011; Curnis et al., 2000) or the labeling of such derivative with ^{64}Cu (Chen et al., 2013) or ^{68}Ga (Zhang et al., 2014; Shao et al., 2014a) (PET-imaging) or with ^{99m}Tc (Ma et al., 2013; Ma et al., 2014) (SPECT-imaging) can serve as useful radiotracers for the *in vivo* imaging of CD13-expression of tumors and neovasculature by binding to APN. Moreover, NGR based radioligands beside the diagnostic purpose might also make it feasible to monitor a tumor's response to therapy, which is important to follow the efficacy of the treatment.
Among *in vivo*, functional imaging techniques, Positron Emission Tomography is one of the most sophisticated methods that also makes it possible to detect tumors with high accuracy

and sensitivity followed by easy quantification (Wester 2007). Furthermore, PET-isotope, Ga-68 bears close to ideal physical properties (89% β^+; $t_{1/2}$ = 67.7 min; $E_{av}(\beta^+)$ = 740 keV), easy, on-site accessibility *via* ^{68}Ge/^{68}Ga-generators and offers a well-established complexation chemistry for the labeling of biomolecules (Velikyan 2013; Smith et al., 2013; Banerjee and Pomper 2013). To our knowledge, only a few ^{68}Ga-labeled NGR conjugates were evaluated under preclinical circumstances for CD13-expression-imaging (Zhang et al., 2014; Shao et al., 2014b). As it has been shown that the cyclic form of NGR has approximately ten-fold greater targeting efficacy than linear configurations of the same peptide sequence for targeting different tumors (Colombo et al., 2002), a cyclic NGR motif containing radiotracer might lead to high diagnostic efficiency. On the other hand, in order to create a ^{68}Ga-labeled c(NGR) conjugate a chelator other than DOTA with the ability to efficiently chelate trivalent gallium-ion at room temperature must be chosen, as thermal stability of a DOTA-c(NGR) conjugate might be insufficient due to decomposition of the cycle or the elevated temperature can enhance the conversion of asparagine residue into isoaspartate and aspartate resulting in isoDGR and DGR sequence (Curnis et al., 2008).

In present study, we intended to combine the advantages of the high affinity of cyclic NGR peptide with simple, room-temperature ^{68}Ga-labeling of 1,4,7-triazacyclononane-1,4,7-triacetic acid (NOTA) to create a highly specific radiotracer for the detection of CD13-positive tumors. For homing devices, c[KNGRE]-NH_2 (cyclic(lysine-asparagine-glycine-arginine-glutamic acid amide)) cyclic peptide (Negussie et al., 2010) was selected in this study because of its significantly higher stability against deamidation compared to cyclic NGR peptides with disulfide bridge. (The comparison of stability of cyclic NGR peptides will be published in a following study). In addition, PET-imaging properties of the new tracer were compared to commercially available, ^{68}Ga-labeled NODAGA-RGD dimer acetate on the very same syngenic, rat tumor models (Trencsenyi et al., 2009; Rozsa et al., 2009) with the potential of showing these tracers capability for metastasis detection in order to further test the utility of ^{68}Ga-NOTA-c(NGR).

2. Materials and Methods

2.1. Chemicals

All commercially available chemicals were of analytical grade and used without further purification. All amino acid derivatives for peptide synthesis were purchased from Reanal (Budapest, Hungary) and IRIS Biotech GmbH (Marktredwitz, Germany), while solvents for synthesis and purification were obtained from Molar Chemicals Kft (Budapest, Hungary). For the radiolabeling studies, Ultrapur® water, HCl and NaOH were obtained from Merck. All other chemicals were the product of Sigma-Aldrich Co. (St. Louis, MO, USA), if not specifically stated otherwise.

2.2. Synthesis of c[KNGRE]-NH_2 cyclic peptide with amide bond

Linear semi-protected H-Lys(ClZ)-Asn-Gly-Arg-Glu-NH_2 was prepared manually by Fmoc/^{t}Bu strategy on Rink-Amide MBHA resin (0.52 mmol/g capacity). Standard Fmoc-amino acid derivatives were used for the synthesis except Boc-Lys(ClZ)-OH that was attached to the N-terminus of the peptide. The semi-protected peptide was cleaved from the resin using a mixture of 95 % TFA, 2.5 % TIS and 2.5 % water (v/v/v) for 3 h at room temperature and then precipitated and washed three times with ice-cold diethyl ether. The product was dissolved in 100 % acetic acid and freeze dried. The crude peptide was purified by semi-preparative RP-HPLC followed by counter ion exchange of TFA to chloride using pyridinium hydrochloride prior cyclization. The semi-protected linear peptide was cyclized in DMF at 0.2 mg/mL peptide concentration in the presence of BOP/HOBt/DIEA (6:6:12 equiv to the peptide) reagents at RT for 24 h. The solvent was evaporated and the remaining oily product was dissolved in eluent A and purified by RP-HPLC. After lyophilization the purified product was dried further in dessiccator over P_2O_5 and then the ClZ group from the side chain of Lys residue was removed with liquid HF (HF – *p*-cresol = 10 mL : 1 g). The crude product was purified by semi-preparative RP-HPLC and analyzed by analytical HPLC, as described below. Identification was performed with ESI-MS (Esquire 3000+ ion trap mass spectrometer Bruker Daltonics, Bremen, Germany).

2.3. Conjugation reaction of c[KNGRE]-NH_2 peptide with *p*-SCN-Bn-NOTA

11.7 mg (20 μmol) from the cyclic pentapeptide c[KNGRE]-NH_2 was dissolved in 0.9 mL of 0.1 M sodium carbonate buffer (pH 9.5). 12.3 mg (22 μmol) of *p*-SCN-Bn-NOTA (Macrocycles Inc., Dallas, TX, USA) was dissolved in 0.1 mL DMSO, and was introduced to the aqueous phase. The mixture was stirred for 2 h at room temperature. The resulting NOTA-conjugated NGR analogue (NOTA-c(NGR)) was purified by means of semi-preparative RP-HPLC and the collected fractions were lyophilized. The pure product was characterized by analytical RP-HPLC (as described below) and ESI-MS (Shimadzu LCMS IT-TOF Mass Spectrometer, Shimadzu Corp., Tokyo, Japan).

2.4. Radiolabeling of NODAGA-[c(RGD)]$_2$ with Ga-68

NODAGA-[c(RGD)]$_2$ was purchased from ABX GmbH (Radeberg, Germany). Labeling was done manually according to the procedure desribed by Notni et al. (2011). Briefly, ^{68}Ga was eluted from a SnO_2-based ^{68}Ge/^{68}Ga-generator (iTHEMBA Labs, Cape Town, South Africa) with 1 M HCl (aq). A fraction of 1250 μl volume containing the highest activity (≈200 MBq) was collected and buffered with 4-(2-hydroxyethyl)-1-piperazineethanesulfonic acid (HEPES; 800 μL, aq, 2.7 M, pH 5.8). Then, 103 μL of a 100 μM NODAGA-[c(RGD)]$_2$ aq. solution was added and and the mixture was let incubate for 5 min at 95°C (pH=3.0). Afterwards, the reaction mixture was transferred onto the surface of an Empore® C18 SD 7mm/3mL Extraction Disc Cartridge. (The cartridge was previously activated applying a 500 μL EtOH and then a 10 mL water wash.) After binding reacted materials from the mixture, the surface was washed with 15 mL water and then retained activity was eluted with 500 μL EtOH/0.9 % NaCl (1:1) – solution. From the eluate, EtOH-content was evaporated in approx. 5 min under 60 mL/min He flow and at 95°C. Final volume was completed to 250 μL with water in order to gain an isotonic final product for further use. Radiochemical purity (%) of the final product was determined by applying an HPLC method described below.

2.5. Radiolabeling of NOTA-c(NGR) with Ga-68

This labeling protocol is based on the procedure desribed by Wängler et al. (2011). Previously mentioned ^{68}Ge/^{68}Ga-generator was eluted with 1 M HCl (aq). A fraction of 1 mL volume containing the highest activity (≈160 MBq) was collected, buffered with sodium-acetate (1M;

1 mL, aq.) and the pH of the stock solution was adjusted to ~ 4.5 by the addition of sodium-hydroxide (10 %, 0.2 mL, aq.). Then, 15 µL of a 1 mM NOTA-c(NGR) aq. solution was added and the mixture was let incubate for 5 min at room temperature. Afterwards, the reaction mixture was transferred dropwise onto the surface of a pre-activated Empore® C18 SD 7mm/3mL Extraction Disc Cartridge. After binding reacted materials from the mixture, the surface was washed with 5 mL water and then retained activity was eluted with 0.35 mL EtOH. From the eluate, solvent was evaporated to dryness in approx. 5 min under 60 mL/min He flow. The labeled peptide was re-dissolved in 250 µL with isotonic saline solution for further use. Radiochemical purity (%) of the final product was determined by applying an HPLC method described below.

2.6. Reversed Phase High Performance Liquid Chromatography (RP-HPLC) methods

For the synthesis of c[KNGRE]-NH_2 peptide, the crude products and the conjugates were purified on a KNAUER 2501 HPLC system (KNAUER, Bad Homburg, Germany) using a semi-preparative Phenomenex Luna C18 column (250 mm x 10 mm) with 10 µm silica (100 Å pore size) (Phenomenex Inc., Torrance, CA, USA). Linear gradient elution (0 min 5 % B; 5 min 5 % B; 50 min 50 % B) with eluent A (0.1% TFA in water) and eluent B (0.1% TFA in MeCN-H_2O (80:20, v/v)) was used at a flow rate of 4 mL/min. Peaks were detected at 220 nm. In this case, analytical RP-HPLC was performed on the same instrument using a Phenomenex Luna C18 column (250 mm x 4.6 mm) with 5 µm silica (100Å pore size) as a stationary phase. Linear gradient elution (0 min 0 % B; 5 min 0 % B; 50 min 90 % B) using the same eluents was applied at a flow rate of 1 mL/min. Peaks were detected at 214 nm.

The purification of the NOTA-conjugated NGR analogue was performed on a KNAUER HPLC system using a semi-preparative Supelco Discovery® Bio Wide Pore C18 column (150 mm x 10 mm) with 10 µm silica with a flow rate 4 mL/min. After a short isocratic period (3 min) a linear gradient was used (3 min 5 % B; 25 min 65 % B) with eluent A (0.1% TFA in water) and eluent B (0.1% TFA in MeCN-H_2O (95:5, v/v), applying 254 nm for peak detection.

For the quality control of the radiolabeled peptides, in comparison with the NOTA-c(NGR) conjugate purification, a similar configuration and the same eluents were used on the previously mentioned KNAUER HPLC system with an analytical Supelco Discovery® Bio Wide Pore C18 column (250 mm x 4.6 mm) with 10 µm silica and 1.2 mL/min flow rate, with

a gradient profile: 0 min 0% B, 3 min 0 % B; 14 min 40 % B. Signals were simultaneously detected by radiodetector and UV detector (254 nm).

2.7. Determination of partition coefficient of ^{68}Ga-NOTA-c(NGR)

The partition coefficient of ^{68}Ga-NOTA-c(NGR) was expressed as log*P* by measuring the distribution of radioactivity in 1-octanol and PBS-solution. Approximately 1.5 MBq of ^{68}Ga-NOTA-c(NGR) in 10 µL aq. solution was added to an Eppendorf-vial containing 0.5 mL of PBS (pH = 7.4) and 0.5 mL of 1-octanol. After vortexing the mixture for 20 min vigorously, the vial was centrifuged at 20,000 rpm for 5 min in order to reach complete separation of layers. 100 µL of each layer was pipette into test tubes; the radioactivity was measured with a gamma counter (Perkin-Elmer Packard Cobra, Waltham, MA, USA). Log*P* value was determined from the results of six experiments.

2.8. Determination of *in vitro* stability of ^{68}Ga-NOTA-c(NGR)

The stability of ^{68}Ga-NOTA-c(NGR) was tested in PBS at 95ºC and in rat serum at 37ºC. Approximately 8 MBq of ^{68}Ga-NOTA-c(NGR) was pipetted into 0.5 mL PBS or into rat serum and was incubated at the respective temperature. For 95ºC study, an aliquot of the solution was directly transferred to reversed-phase HPLC testing (as described above) for the determination of radiochemical purity at various time points (0, 5, 30 and 60 min). For rat serum stability study, at various time points (0, 30, 60, 90 and 120 min) a 50 µL aliquot of the stock solution was mixed with 50 µL cold abs. EtOH. Precipitated fraction was separated by centrifugation at 20,000 rpm for 5 min. The supernatant was collected, further diluted with water and transferred to reversed-phase HPLC testing (as method prescribed above) for the determination of radiochemical purity.

2.9. Animals

Animals (Fischer-344 rats) were housed under conventional conditions in air conditioned rooms at a temperature of 26±2°C, with 50±10% humidity and artificial lighting with a circadian cycle of 12 h. The semi-synthetic diet (Charles River Hungary Ltd., Gödöllő, Hungary) and drinking water were available ad libitum to all the animals. The animals received human care complying with the criteria outlined in the “Guidelines for the welfare

and use of animals in cancer research" (Workman et al., 1988), authorized by the Ethical Committee for Animal Research, University of Debrecen, Hungary (permission number: 22/2007). Laboratory animals were kept and treated in compliance with all applicable sections of the Hungarian Laws No. XXVIII/1998 and LXVII/2002 on the protection and welfare of animals and animal welfare directions and regulations of the European Union.

2.10. Experimental tumor

Chemically induced rat mesenchymal mesoblastic nephroma (NeDe) tumor was used in our experiments (Trencsenyi et al., 2009; Rozsa et al., 2009). The experimental renal tumor was isolated from Fischer 344 rats which had been treated at newborn age by the *i.p.* injection of 125 μg/animal *N*-nitrosodimethylamine in saline. Tumors were removed 5–7 months after chemical tumorogenesis, minced into smaller pieces, then the tumor slices were frozen (Dezso et al., 1991) and the NeDe cell line was established (Rozsa et al., 2009).

2.11. Tumor models

Adult male Fischer-344 rats (n=20) weighing 200–250 g were used for tumor-transplanted animal experiments. For the subcutaneous animal model $5x10^6$ NeDe tumor cells in 150 μl saline were injected subcutaneously into the left thighs. Tumor growth was assessed by caliper measurements and tumor size was calculated using the following formula: (largest diameter x smallest diameter^2)/2. The *in vivo* experiments were carried out 12±2 days after subcutaneous injection of tumor cells when the tumor volume was 1.5±0.24 cm^3. For the induction of another tumor model the subrenal capsule assay (SRCA) was used. The aim of this surgical operation was to place Gelaspon® discs (Germed, Rudolstadt, Germany) containing tumor cells under the capsule of the left kidney. For this transplantation, $5x10^6$ NeDe tumor cells in 20 μl saline were placed on a Gelaspon® disc (Trencsenyi et al., 2009). Animals were anaesthetized by 3% isoflurane with a dedicated small animal anesthesia device and the retroperitoneum was opened by abdominal section, the left kidney was exposed and the Gelaspon® disc containing tumor cells was placed under the renal capsule. Stitches were put in the wound and the tumors were allowed to grow until 1.4-1.6 cm^3 and *in vivo* experiments were carried out.

2.12. Small animal PET imaging using radiopharmaceuticals

12±2 days after the implantation of NeDe cells control and tumor-bearing rats were injected *via* the tail vein with 7.4±0.2 MBq of ^{68}Ga-NOTA-c(NGR) or ^{68}Ga-NODAGA-[c(RGD)]$_2$. 90 min after tracer injection animals were anaesthetized by 3% isoflurane with a dedicated small animal anesthesia device and whole body PET scans (10-min static PET scans at each bed position) were acquired using the MiniPET-II small animal PET scanner (Lajtos et al., 2013). The MiniPET-II scanner consists of 12 detector modules including LYSO scintillator crystal blocks and position sensitive PMTs. Each crystal block comprises 35 x 35 pins of 1.27 x 1.27 x 12 mm size. Detector signals are processed by FPGA based digital signal processing boards with embedded Linux operating system. Data collection and image reconstruction are performed using a data acquisition module with Ethernet communication facility and a computer cluster of commercial PCs. Scanner normalization and random correction were applied on the data and the images were reconstructed with the standard EM iterative algorithm. The pixel size was 0.5x0.5x0.5 mm and the spatial resolution varies between 1.4 to 2.1 mm from central to 25 mm radial distances. The system sensitivity is 11.4%. For the determination of the anatomical localization of the tumors, CBCT (3D Accuitomo, XYZ Slice View Tomograph, I. Morita MFG. Corp, Kyoto, Japan) was used. The X-ray tube settings were voltage 60 kVp, current 8.0 μA, and exposure time 30.8 s per projection; voxel size: 160 μm.

2.13. PET data analysis

Radiotracer uptake was expressed in terms of standardized uptake values (SUVs) and tumor to muscle (T/M) ratios. Ellipsoidal 3-dimensional volumes of interest (VOI) were manually drawn around the edge of the tumor activity by visual inspection using BrainCad software (http:/www.minipetct.hu). The standardized uptake value (SUV) was calculated as follows: SUV = [ROI activity (Bq/mL)]/[injected activity (Bq)/animal weight (g)], assuming a density of 1 g/mL. The T/M ratios were computed as the ratio between the activity in the tumor VOI and in the background (muscle) VOI.

2.14. *Ex vivo* organ distribution studies

One day after PET scans, control and tumor-bearing experimental animals were anaesthetized and 7.4±0.2 MBq of ^{68}Ga-NOTA-c(NGR) (approx. 1.9 μg peptide/animal) or ^{68}Ga-NODAGA-[c(RGD)]$_2$ (approx. 3 μg peptide/animal) were injected *via* the tail vein. After the incubation time (90 min) rats were euthanized with the intraperitoneal injection of 60 mg/kg pentobarbital (Nembutal) and blood samples were taken from the heart. Three tissue samples were taken from each organ (liver, spleen, kidneys, intestine, heart, stomach, muscle, lung and tumor) and their activities were measured with a calibrated gamma counter (Perkin-Elmer Packard Cobra, Waltham, MA, USA). The weight and the radioactivity of the samples were used to determine the differential absorption ratio (DAR). DAR value was calculated as:

$$DAR = \frac{\text{(accumulated radioactivity/g tissue)}}{\text{(total injected radioactivity/body weight)}}$$

2.15. Blocking experiments

For the *ex vivo* and *in vivo* blocking experiments, control and NeDe tumor-bearing rats were pretreated with 200 μg unlabeled NOTA-c(NGR) in 100 μL saline (as a blockade, approx. 100 fold of the ^{68}Ga-labeled peptides) by intravenous injection 5 minutes prior to administration of ^{68}Ga-NOTA-c(NGR). 90 min after the injection of the ^{68}Ga-labeled tracer *ex vivo* and *in vivo* biodistribution studies were performed as described above.

2.16. Western blot analysis

Cells were harvested in lysis buffer (20 mM Tris-HCl, pH 7.4, 5 mM EGTA, 1 mM 4-(2-aminoethyl)benzensulfonyl fluoride, protease inhibitor cocktail diluted 1:100, while frozen tissue samples were pulverized under liquid nitrogen with a mortar and pestle and the resulting powder was subsequently dissolved in the lysis buffer mentioned above. After sonication the protein content of the resulting samples was determined by a modified BCA protein assay (Pierce Protein Biology Products, Thermo Fisher Scientific Inc., Rockford, IL,

USA). The samples were then subjected to sodium dodecyl sulfate-polyacrylamide gel electrophoresis (10% gels were loaded with equal [20-60 μg] amount of protein per lane), transferred to BioBond nitrocellulose membranes (Whatman, GE Healthcare Bio-Sciences AB, Uppsala, Sweden), and then probed with mouse-anti-rat CD13 (from Santa-Cruz Biotechnology Inc. (Dallas, TX, USA**)**; 1:100 dilution in 5% milk containing PBS). As secondary antibodies, horseradish peroxidase-conjugated mouse IgG Fc segment-specific antibodies (developed in goat, 1:1000, Bio-Rad Laboratories, Inc. (Hercules, CA, USA) was used, and the immunoreactive bands were visualized by a SuperSignal® West Pico Chemiluminescent Substrate enhanced chemiluminescence kit (Pierce Protein Biology Products) using a KODAK Gel Logic 1500 Imaging System (Eastman Kodak Company, Rochester, NY, USA). To assess equal loading, when indicated, membranes were re-probed with anti-β-actin antibodies (1:1000 dilution in 5% milk containing PBS) and visualized as described above.

2.17. Statistical analysis

Data are presented as mean ± SD of at least three independent experiments. The significance was calculated by Student's t test (two-tailed). The significance level was set at $p \leq 0.05$ unless otherwise indicated.

3. Results

3.1. Chemical and radiochemical synthesis

First synthetic steps of the targeting peptide were performed successfully with a 49% calculated cyclization yield and an almost quantitative protecting group cleavage. Purity of the final NGR analogue (c[KNGRE]-NH_2) was found to be 98%< by means of analytical HPLC and was identified to be $[M+2H]^{2+}$ = 292.9 and $[M+H]^{+}$ = 584.4 by ESI-MS. Similarly, the resulting product of the conjugation reaction of *p*-SCN-Bn-NOTA and c[KNGRE]-NH_2 (isolated yield: 73%) was analyzed by analytical HPLC (purity 98%<), while the identification by ESI-MS found it $[M+2H]^{2+}$ = 517.75, as expected. Reaction scheme of the chemical synthesis of NOTA-c(NGR) can be seen on Fig. 1A. Labeling procedures of NOTA-c(NGR) and commercially available NODAGA-$[c(RGD)]_2$ was performed in 30 min with a decay-corrected yield in the range of 65-75 %, a radiochemical purity of 95%< and a specific activity of 5.13 – 5.92 GBq/μmol for ^{68}Ga-NOTA-c(NGR) and 9.34 – 10.77 GBq/μmol for ^{68}Ga-NODAGA-$[c(RGD)]_2$ at all cases. All labeled tracers were used directly for further experiments after formulation. The chemical structure of ^{68}Ga-NODAGA-$[c(RGD)]_2$ and newly synthesized ^{68}Ga-NOTA-c(NGR) can be seen on Fig. 1B and C.

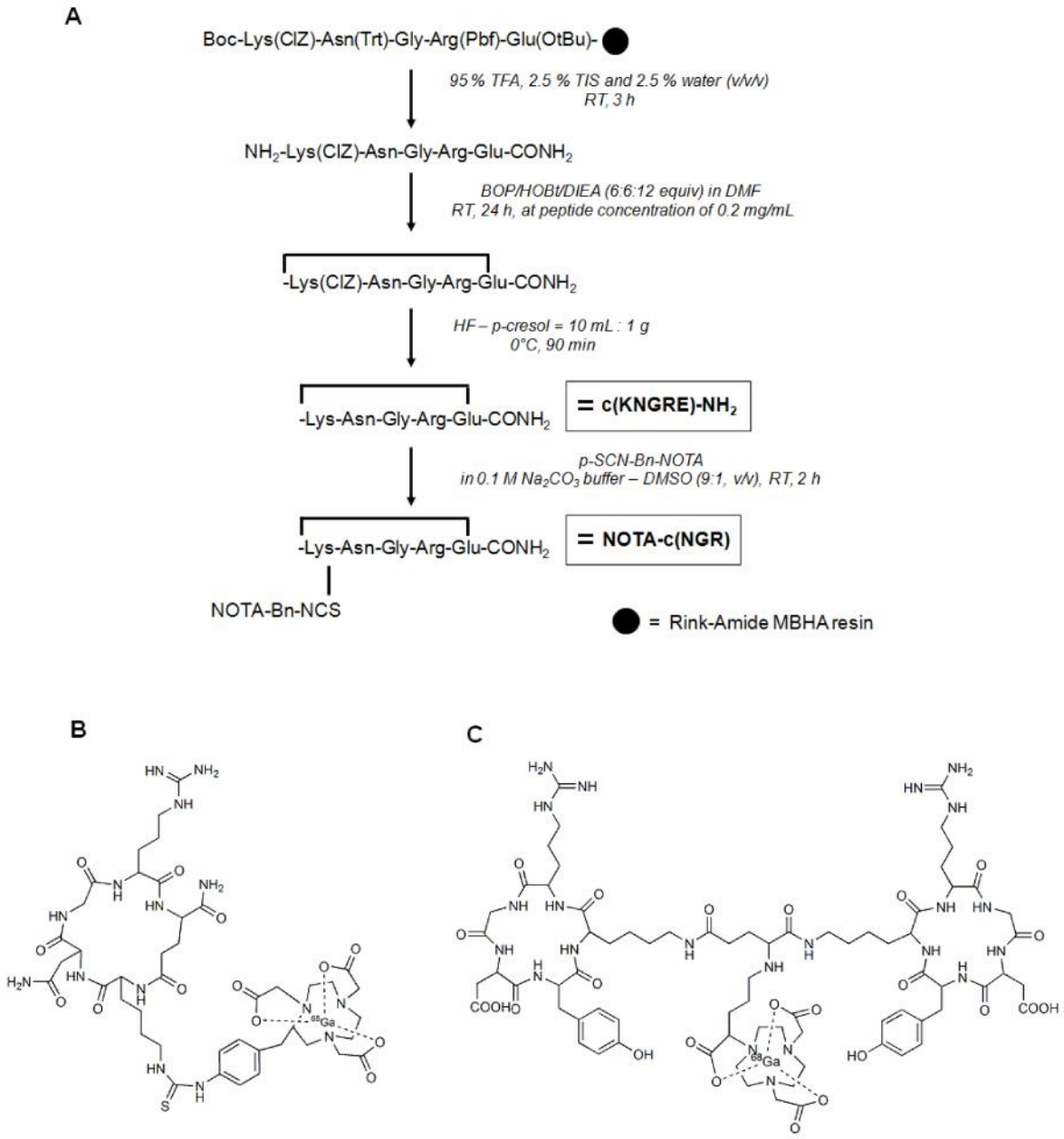

Fig. 1. Reaction scheme of the chemical synthesis of NOTA-c(NGR) (A), chemical structure of ^{68}Ga-NOTA-c(NGR) (B) and ^{68}Ga-NODAGA-[c(RGD)]$_2$ (C).

3.2. Partition coefficient and *in vitro* stability of ^{68}Ga-NOTA-c(NGR)

The partition coefficient (log*P*) of ^{68}Ga-NOTA-c(NGR) was determined to be – 2.77 ± 0.12, suggesting that the radiotracer is highly hydrophilic. Also, stability of the labeled peptide was measured in rat serum at 37ºC and at increased temperature (PBS; pH = 7.4; T = 95ºC) by

means of analytical radio-HPLC. After 2 hours of incubation in rat serum, more than 95 % of the original labeled peptide was found to be intact; also at increased temperature first signs of degradation was observed only at 1 hour, when still 98%< radiochemical purity was found. These latter results suggest a highly stable molecule under the applied conditions in the following experiments.

3.3. *In vivo* and *ex vivo* biodistribution studies on healthy animals

In vivo and *ex vivo* biodistribution studies were performed using healthy Fischer-344 rats as controls. 90 min after the injection of 7.4±0.2 MBq of ^{68}Ga-NOTA-c(NGR) or ^{68}Ga-NODAGA-[c(RGD)]$_2$ the biodistributions were evaluated by whole body miniPET scans. The representative decay-corrected coronal miniPET/CT images are shown in Fig. 2A. In the animals injected with ^{68}Ga-NODAGA-[c(RGD)]$_2$ the high uptake of the liver, spleen and intestines were clearly visualized. In contrast, moderate accumulation was observed in the animals injected with ^{68}Ga-NOTA-c(NGR) Fig. 2B.

This *in vivo* biodistribution results correlated well with the *ex vivo* data. For the *ex vivo* studies the animals were sacrificed 90 min after the tracer injection, dissected, and the accumulated activity of the tissues and organs was counted with a gamma counter. The results are summarized in Fig. 2C; 90 min after the injection of ^{68}Ga-NOTA-c(NGR) the DAR values of kidneys and urine showed high tracer accumulation in control rats. In contrast with these result, the liver, intestines, spleen and stomach showed significantly higher ($p \leq 0.01$) uptake after the injection of ^{68}Ga-NODAGA-[c(RGD)]$_2$.

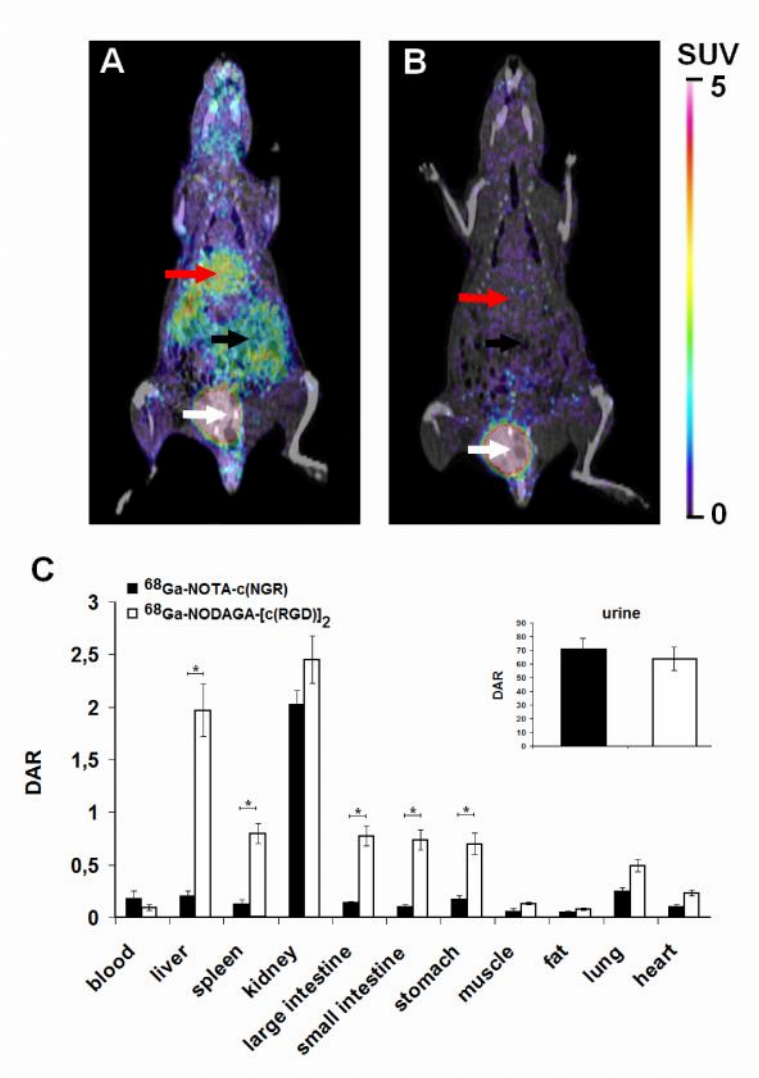

Fig. 2. Comparison of *in vivo* and *ex vivo* biodistribution data for ^{68}Ga-NOTA-c(NGR) (n=5) and ^{68}Ga-NODAGA-[c(RGD)]$_2$ (n=5). A: Representative coronal miniPET/CT image of control F-344 rats 90 min after the injection of ^{68}Ga-NODAGA-[c(RGD)]$_2$. B: Representative coronal miniPET/CT image of control F-344 rats 90 min after the injection of ^{68}Ga-NOTA-c(NGR). Red arrows: liver, white arrows: urine, black arrow: intestines. C: quantitative analysis of tracer uptake in control animals 90 min after the injection of ^{68}Ga-NOTA-c(NGR) and ^{68}Ga-NODAGA-[c(RGD)]$_2$. DAR values are presented as mean±SD; significance level: $p \leq 0.01$ (*).

Ex vivo blocking studies were performed on healthy animals as described in *Materials and methods (see 2.15. Blocking experiments)*. Results are summarized in Table 1, where the DAR values of the examined organs can be seen. The ^{68}Ga-NOTA-c(NGR) uptake of the organs or tissues was lower after the injection of 200 µg unlabeled NOTA-c(NGR). The radiotracer

uptake in the selected organs was approximately two-fold higher without the blockade (Table 1).

Table 1

Tracer uptake (DAR) in selected organs/tissues 90 min after tracer injection

Organ/tissue	^{68}Ga-NOTA-c(NGR) (n=5)	^{68}Ga-NOTA-c(NGR) blocked (n=5)
blood	0.17 ± 0.08	0.12 ± 0.2
liver	0.21 ± 0.05	0.10 ± 0.01
spleen	0.13 ± 0.04	0.08 ± 0.01
kidney	2.02 ± 0.13	1.39 ± 0.04
large intestine	0.14 ± 0.01	0.07 ± 0.01
small intestine	0.10 ± 0.02	0.04 ± 0.02
stomach	0.17 ± 0.04	0.05 ± 0.02
muscle	0.05 ± 0.02	0.02 ± 0.01
fat	0.04 ± 0.01	0.02 ± 0.01
lung	0.24 ± 0.03	0.10 ± 0.04
heart	0.10 ± 0.01	0.04 ± 0.02

3.4. *In vivo* and *ex vivo* biodistribution studies on subcutan tumor model

The tumor targeting efficacy of ^{68}Ga-NOTA-c(NGR) and ^{68}Ga-NODAGA-[c(RGD)]$_2$ in NeDe tumor-bearing F-344 rats was compared by miniPET scans 90 min after tracer injection. Representative decay-corrected axial images are shown in Fig. 3. The subcutaneously growing NeDe tumors were clearly visualized with ^{68}Ga-NOTA-c(NGR) (Fig. 3B) with high tumor-to-muscle (T/M) ratios (Fig. 3C), where the T/M SUVmean, and the T/M SUVmax were 12.25±3.08 and 16.28±2.48, respectively. These ratios approximately two-fold higher than that of the ^{68}Ga-NODAGA-[c(RGD)]$_2$ uptake, where the T/M SUVmean and the T/M SUVmax were 6.39±0.38 and 7.8±1.14, respectively.

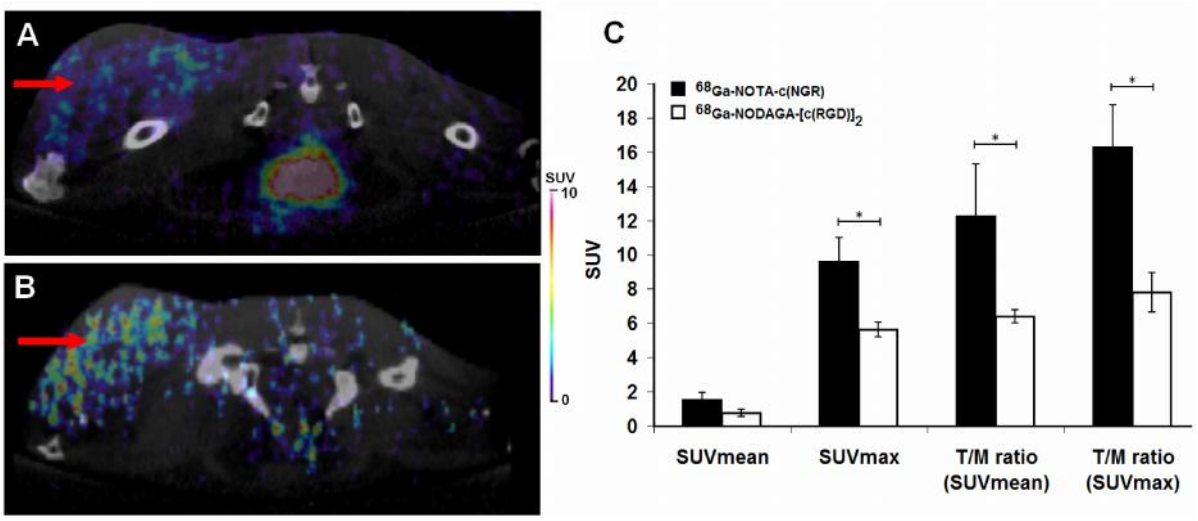

Fig. 3. Comparison of *in vivo* biodistribution of ^{68}Ga-NODAGA-[c(RGD)]$_2$ and ^{68}Ga-NOTA-c(NGR) 12±2 days after subcutaneous injection of NeDe cells. Representative axial miniPET/CT images of the same subcutaneously growing NeDe tumors (red arrows) 90 min after the injection of ^{68}Ga-NODAGA-[c(RGD)]$_2$ (A) and ^{68}Ga-NOTA-c(NGR) (B). C: quantitative analysis of the tracer uptake in NeDe tumors (n=6). Significance level: $p \leq 0.01$ (*).

To investigate the Aminopeptidase N (APN/CD13) specificity of ^{68}Ga-NOTA-c(NGR) in subcutaneously growing NeDe tumors, we performed *in vivo* biodistribution studies at 90 min post injection with or without a blocking dose of 200 µg unlabeled NOTA-c(NGR). Fig. 4 demonstrates that the unlabeled NOTA-c(NGR) significantly ($p \leq 0.01$) reduced the uptake of ^{68}Ga-NOTA-c(NGR) in NeDe tumors (Fig. 4B and C). By taking the SUV values, the SUVmean, SUVmax, T/M SUVmean and T/M SUVmax the tracer accumulation in the tumors was blocked efficiently and dropped to 0.35±0.22, 2.26±0.43, 2.50±0.39 and 2.48±1.14, respectively, confirming the CD13 binding specificity *in vivo*.

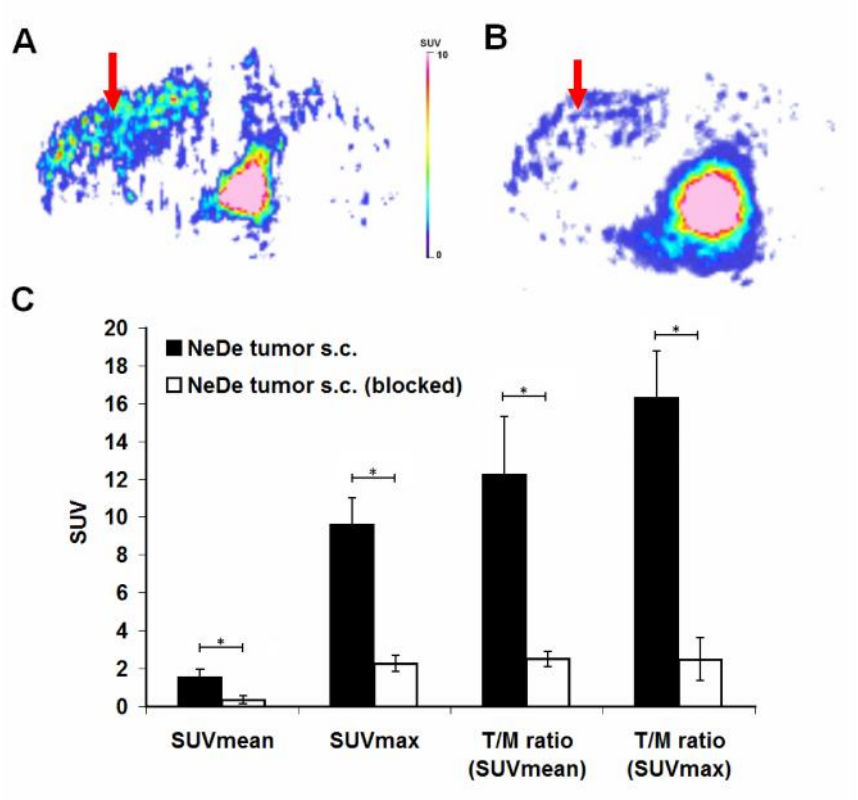

Fig. 4. Upper row: Representative axial miniPET images of the same NeDe tumor 90 min after the injection of ^{68}Ga-NOTA-c(NGR) and 12 days after subcutaneous injection of NeDe cells. A: base, B: blocked *(see 2.15. Materials and methods)*. Red arrows: tumor. C: Quantitative analysis of *in vivo* tracer uptake data (90 min post inj.) in *s.c.* NeDe tumors for ^{68}Ga-NOTA-c(NGR) (n=5) in comparison with data obtained for ^{68}Ga-NOTA-c(NGR) blocking (n=6) experiments 12±2 days after subcutaneous injection of tumor cells. Significance level: $p \leq 0.01$ (*).

These miniPET results correlated with the *ex vivo* bidistribution data where the *s.c.* NeDe tumor-bearing rats were sacrificed 90 min after the tracer injection, dissected, and the accumulated activity of the tumors and muscle (as background) was counted with a gamma counter and DAR values were calculated. The results are summarized in Table. 2.

Table 2

Tracer uptake (DAR) in *s.c.* NeDe tumors 90 min after tracer injection

Organ/tissue	^{68}Ga-NODAGA-[c(RGD)]$_2$ (n=5)	^{68}Ga-NOTA-c(NGR) (n=5)	^{68}Ga-NOTA-c(NGR) blocked (n=6)
NeDe tumor (*s.c.*)	0.34 ± 0.08	0.37 ± 0.08	0.07 ± 0.02
Tumor/muscle	3.66 ± 1.23	7.42 ± 2.27	1.23 ± 0.06

3.5. *In vivo* and *ex vivo* biodistribution studies on the SRCA tumor model

The accumulation of ^{68}Ga-NOTA-c(NGR) and ^{68}Ga-NODAGA-[c(RGD)]$_2$ in NeDe tumors growing under the left renal capsule was compared by miniPET scans 90 min after tracer injection. Decay-corrected representative coronal images are shown in Fig. 5. NeDe tumors growing under the renal capsule were clearly visualized with both radiotracers (Fig. 5A and B). No significant differences (at $p \leq 0.05$ level) were found in the SUV mean values of the tumors: SUVmean of ^{68}Ga-NOTA-c(NGR) and ^{68}Ga-NODAGA-[c(RGD)]$_2$ was 1.73±0.39 and 1.31±0.24, respectively. However, significant differences ($p \leq 0.01$) were found when SUVmax and T/M SUVmax values were compared (Fig. 5C), where the SUVmax and the T/M SUVmax values of ^{68}Ga-NOTA-c(NGR) uptake were 11.47±1.37 and 12.47±2.19, respectively. These values approximately two-fold higher than that of the ^{68}Ga-NODAGA-[c(RGD)]$_2$ uptake, where the SUVmax and the T/M SUVmax were 4.96±0.47 and 6.98±0.55, respectively.

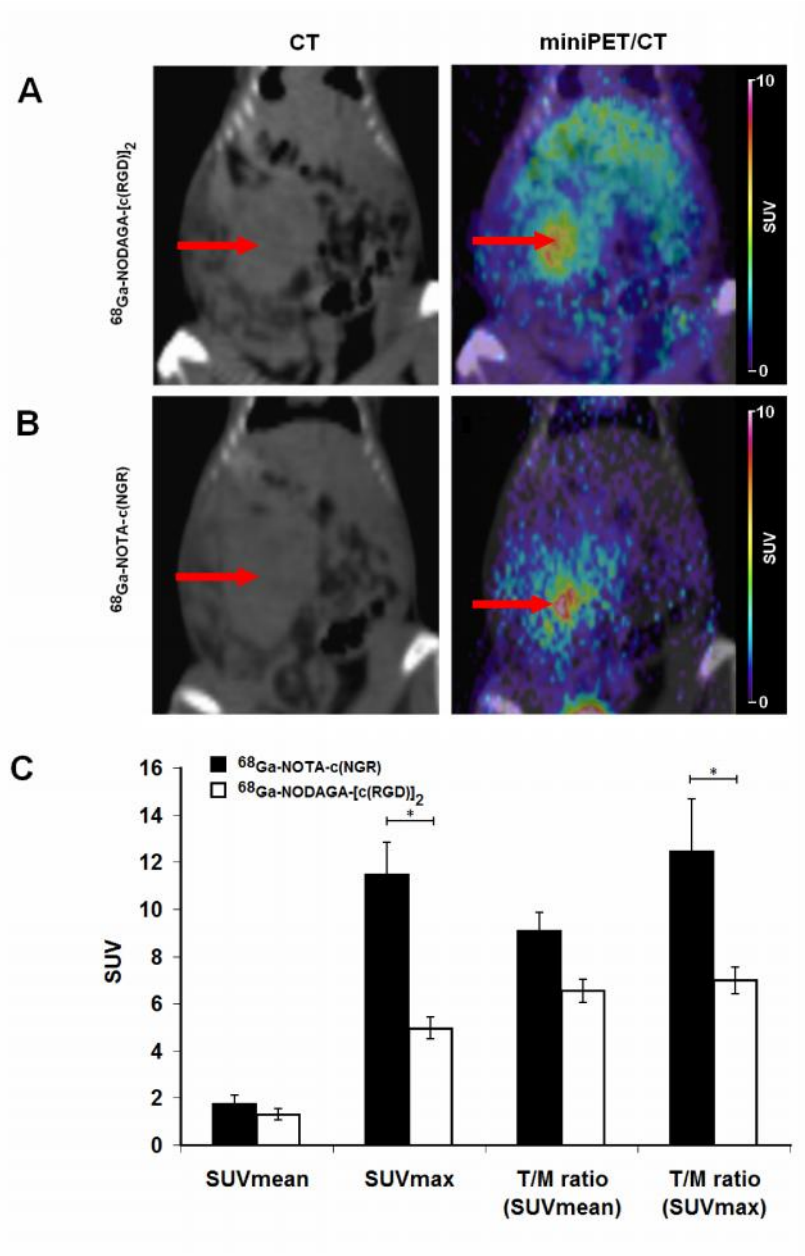

Fig. 5. Comparison of *in vivo* biodistribution of ^{68}Ga-NODAGA-[c(RGD)]$_2$ and ^{68}Ga-NOTA-c(NGR) 12±2 days after SRCA implantation of NeDe cells. Representative coronal CT and miniPET/CT images of NeDe tumors growing under the renal capsule (red arrows) 90 min after the injection of ^{68}Ga-NODAGA-[c(RGD)]$_2$ (A) and ^{68}Ga-NOTA-c(NGR) (B). C: quantitative analysis of the tracer uptake in NeDe tumors (n=6).

The CD13 specificity of ^{68}Ga-NOTA-c(NGR) was also investigated in NeDe tumors growing under the renal capsule. For the blocking experiments we performed *in vivo* miniPET scanning at 90 min post injection with or without a blocking dose of 200 µg unlabeled NOTA-c(NGR), afterwards CT scans were carried out in the same bed position. As can be seen in Fig. 6, the unlabeled NOTA-c(NGR) reduced the uptake of ^{68}Ga-NOTA-c(NGR) in experimental NeDe tumors (Fig. 6B and C). The quantitative analysis of miniPET images (Fig. 6C) showed that the SUV values significantly ($p \leq 0.01$) decreased (SUVmean: 0.63±0.22, SUVmax: 2.8±0.42, T/M SUVmean: 1.71±0.24 and T/M SUVmax: 1.96±0.56) after the injection of unlabeled NOTA-c(NGR), that signed that the tracer accumulation in the tumors was blocked efficiently confirming the CD13 binding specificity.

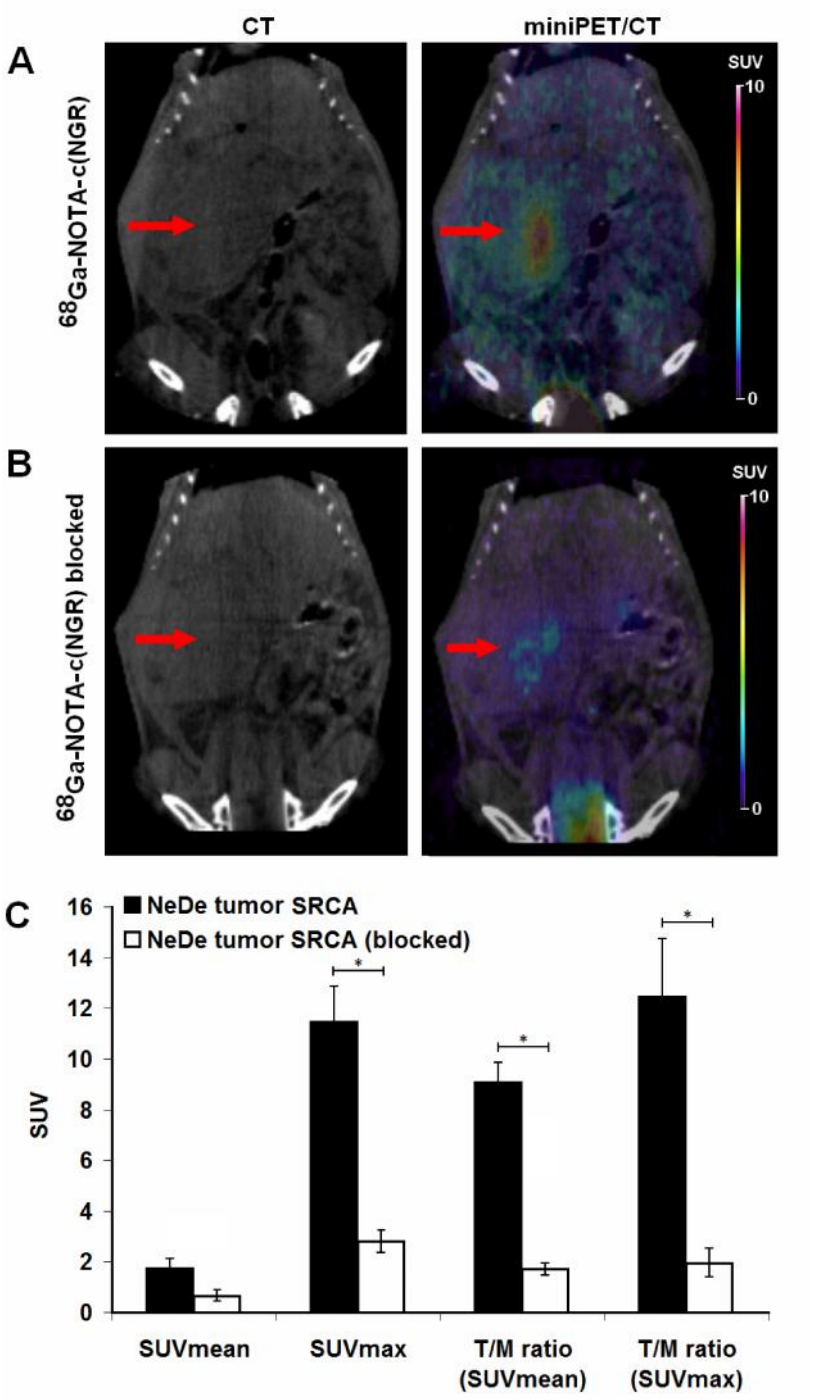

Fig. 6. Representative coronal CT and miniPET/CT images of the same NeDe tumor 90 min after the injection of ^{68}Ga-NOTA-c(NGR) and 12 days after SRCA implantation of NeDe cells. A: base, B: blocked *(see 2.15. Materials and methods)*. Red arrows: tumors (SRCA). C: Quantitative analysis of *in vivo* tracer uptake data (90 min post inj.) in NeDe tumors for ^{68}Ga-NOTA-c(NGR) (n=5) in comparison with data obtained for ^{68}Ga-NOTA-c(NGR) blocking (n=6) experiments. Significance level: $p \leq 0.01$ (*). SRCA: Subrenal Capsule Assay.

The *ex vivo* biodistribution data of the subrenal NeDe tumor bearing rats are summarized in Table 3. Rats were sacrificed 90 min after the tracer injection, dissected and the accumulated activity of the tumors and muscle (as background) was counted with a gamma counter and DAR values were calculated.

Table 3

Tracer uptake (DAR) in SRCA NeDe tumors 90 min after tracer injection

Organ/tissue	^{68}Ga-NODAGA-[c(RGD)]$_2$ (n=5)	^{68}Ga-NOTA-c(NGR) (n=5)	^{68}Ga-NOTA-c(NGR) blocked (n=6)
NeDe tumor (SRCA)	0.54 ± 0.08	0.63 ± 0.18	0.18 ± 0.06
Tumor/muscle	4.39 ± 0.46	6.49 ± 0.21	1.7 ± 0.22

3.6. *In vivo* and *ex vivo* biodistribution studies on metastases

Two weeks after NeDe cell implantation under the left renal capsule metastatic lymph nodes were found in the tumor bearing rats. By autopsy we found that the mesenteric lymph nodes in the abdomen and the parathymic lymph nodes in the thorax showed tumorous infiltration (Fig. 7). The CD13 expression of the metastatic lymph nodes was confirmed by western blot analysis (Fig. 8). The accumulation of ^{68}Ga-NOTA-c(NGR) in the metastatic lymph nodes was investigated by *ex vivo* biodistribution studies after 90 min incubation time. For the blocking experiments 200 μg unlabeled NOTA-c(NGR) was used. By calculating the DAR values we found high ^{68}Ga-NOTA-c(NGR) uptake in the metastatic mesenteric (0.30 ± 0.18) and in the parathymic (0.69 ± 0.24) lymph nodes. In blocking experiments when unlabeled NOTA-c(NGR) was injected 5 min before the ^{68}Ga-labeled radiotracer, the accumulation in the lymph nodes was blocked efficiently confirming the CD13 binding specificity (Fig. 7E).

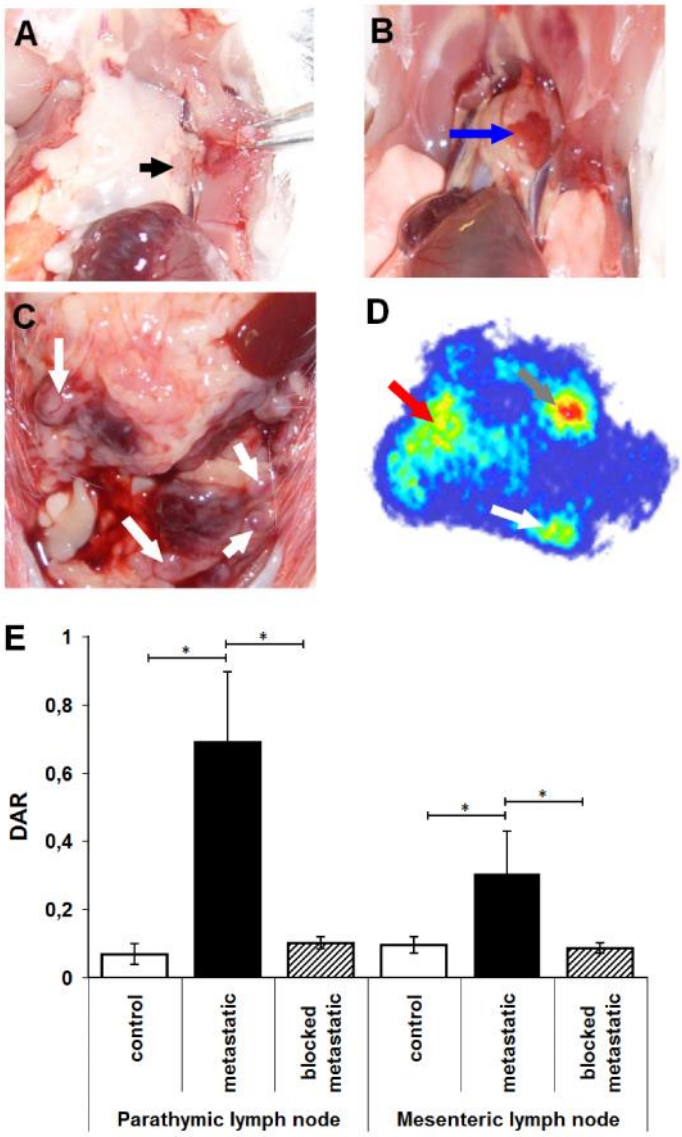

Fig. 7. Assessment of ^{68}Ga-NOTA-c(NGR) uptake in metastatic lymph nodes 12 days after SRCA implantation. A: control parathymic lymph node in the thorax (black arrow), B: metastatic parathymic lymph node (blue arrow), C: metastatic mesenteric lymph nodes (white arrows), D: representative axial miniPET image of a NeDe tumor-bearing rat 90 min after the injection of ^{68}Ga-NOTA-c(NGR) and 12 days after SRCA implantation of NeDe cells (red arrow: primary NeDe tumor, gray arrow: right kidney, white arrow: metastatic mesenteric lymph node), E: Quantitative analysis of *ex vivo* tracer uptake data (90 min post inj.) in NeDe tumors for ^{68}Ga-NOTA-c(NGR) (n=5) in comparison with data obtained for ^{68}Ga-NOTA-c(NGR) blocking (n=6) experiments *(see Materials and methods)*. Significance level: $p \leq 0.01$ (*). SRCA: Subrenal Capsule Assay.

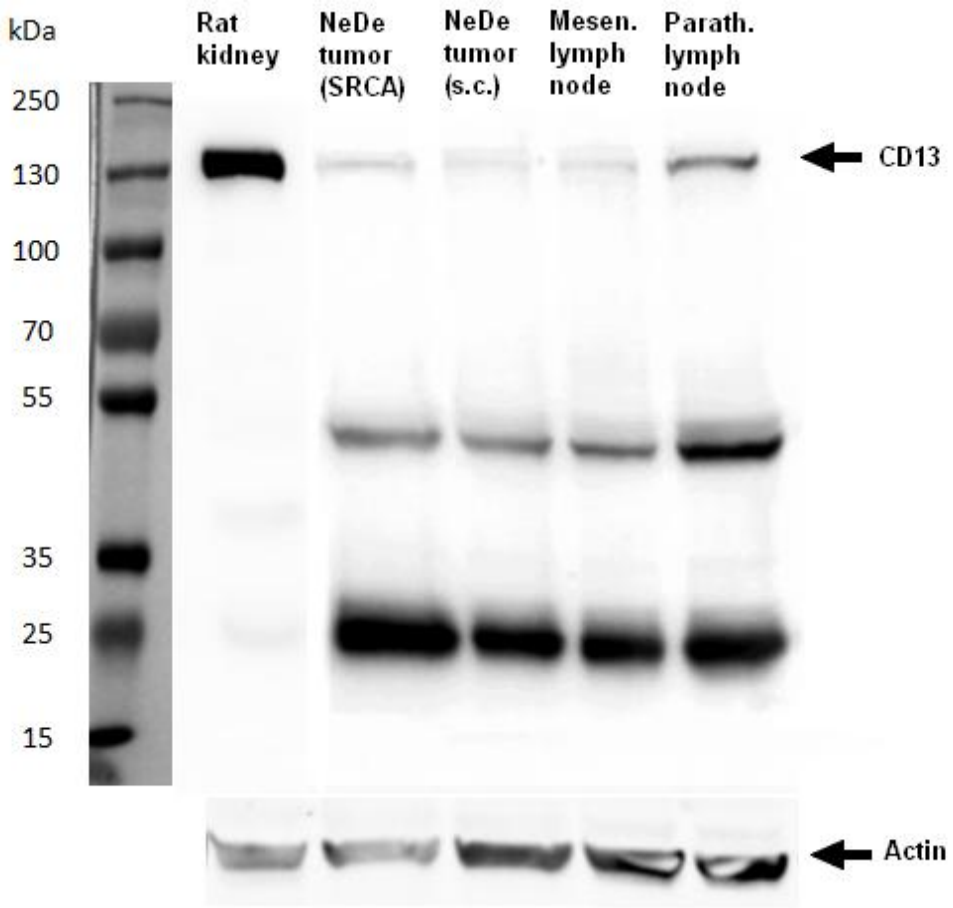

Fig. 8. Western blot analysis of APN/CD13 expression in experimental kidney tumors and lymph node metastases. Rat kidney was used as positive control. SRCA: Subrenal Capsule Assay induced tumor; *s.c.*: subcutan tumor; Mesen. lymph node: Mesenteric lymph node metastasis; Parath. lymph node: Parathymic lymph node metastasis.

4. Discussion

Nowadays, the PET and SPECT imaging of tumor neoangiogenesis with isotope labeled tracers targeting Aminopeptidase N (APN/CD13) and integrin receptors is an intensively investigated field in oncology (Faintuch et al., 2014; Ma et al., 2013, 2014). In this paper, we focused on the PET imaging of APN/CD13 receptor expression in experimental rat tumor models using a new ^{68}Ga labeled radiotracer NOTA-c(NGR).

APN/CD13 is a membrane-associated exopeptidase, involved in the angiogenesis and metastatic process by degradation of extracellular matrix (Su et al., 2012), furthermore, one of the promising tumor associated targets for imaging of cancer and tumor vasculature. In addition, APN/CD13 is a promising target in anti-angiogenic therapy (Yang et al., 2014).

The asparaginyl–glycinyl–arginine (NGR) peptide has been identified as the specific ligand of Aminopeptidase N and has a higher efficacy for the detection of neoangiogenic vessels than the integrin receptor specific RGD peptides (Arap et al., 1998). Several studies have reported that labeling NGR peptide with PET (^{64}Cu, ^{68}Ga) and SPECT (^{99m}Tc) isotopes served useful radiotracers for the *in vivo* imaging of APN receptor expression of tumors and neovasculature by binding to APN (Zhang et al., 2014; Shao et al., 2014b; Ma et al., 2013, 2014).

This current study aimed to investigate newly synthesized ^{68}Ga-NOTA-c(NGR) as a new molecular probe for the evaluation of APN expression in experimental tumors.

The synthesis of the cyclic NGR peptide (c[KNGRE]-NH_2) was developed by Negussie et al. (2010). They prepared the cyclic peptide using on resin cyclization. In this manuscript, we introduced an efficient alternative route for the synthesis of c[KNGRE]-NH_2 cyclic peptide. In this case, the linear protected peptide (Boc-Lys(ClZ)-Asn(Trt)-Gly-Arg(Pbf)-Glu(O^{t}Bu)-R) was built up on solid support by standard Fmoc/^{t}Bu strategy followed by removal of a semi-protected peptide (H-Lys(ClZ)-Asn-Gly-Arg-Glu-NH_2) from the resin using TFA cleavage mixture. The amide bond formation between the N-terminal amino group and the γ-carboxyl group of glutamic acid was carried out in diluted DMF solution by the aid of coupling agents. Prior to the removal of ClZ protecting group with liquid HF, the semi-protected cyclic peptide was purified by RP-HPLC. The cyclic NGR peptide was prepared successfully by the application of this procedure and no deamidation through succinimide ring closure was observed in any stage of the synthesis. As a following step, pure c[KNGRE]-NH_2 peptide was successfully conjugated with *p*-SCN-Bn-NOTA, then the resulting NOTA-c(NGR) was easily labeled afterwards with ^{68}Ga with a RCP of 95%< and a specific activity of 5.13 – 5.92 GBq/μmol with a protocol based on the labeling procedure described by Wängler et al.

(2011). Similarly, the radiosynthesis of ^{68}Ga-NODAGA-[c(RGD)]$_2$ was performed for control experiments with a labeling procedure based on the description of Notni et al. (2011).

The *in vitro* experiments demonstrated that newly synthesized ^{68}Ga-NOTA-c(NGR) is highly hydrophilic (log*P* = – 2.77 ± 0.12) and was also found to be stable both in PBS at increased temperature (T = 95ºC) for 1 hour and in rat serum at 37°C for 2 h; these results demonstrate that ^{68}Ga-NOTA-c(NGR) is an appropriate candidate for further experiments.

Ex vivo and *in vivo* biodistribution studies on control animals revealed that ^{68}Ga-NOTA-c(NGR) was mainly excreted from the kidney, due to its hydrophilic properties that has been proved by the partition coefficient. On the other hand, the uptake of the tracer in other organs was very low, especially in the abdomen (Fig. 2) in contrast to the ^{68}Ga-NODAGA-[c(RGD)]$_2$, where the abdominal organs (liver, spleen, intestines) showed radiotracer uptake after 90 min incubation time (Fig. 2). This moderate accumulation of ^{68}Ga-NODAGA-[c(RGD)]$_2$ in the abdominal organs correlated well with other studies, where the biodistribution of ^{68}Ga-DOTA-NGR (Zhang et al., 2014) and ^{68}Ga-NOTA-NGR (Shao et al., 2014a, 2014b) molecules were investigated. Furthermore, the low activity of other organs also allowed for high quality images with low background and high tumor-to-muscle ratios to be obtained.

In our study, we investigated the tumor specific accumulation of ^{68}Ga-NOTA-c(NGR) as a new molecular probe for imaging angiogenesis-marker expression, comparing with the commercially available $\alpha_v\beta_3$ integrin receptor specific ^{68}Ga-NODAGA-[c(RGD)]$_2$ (Pohle et al., 2012; Beer et al., 2011) on two different animal models using a small animal PET scanner. In this paper, we test different types of administrations of nephroblastoma (NeDe) tumor cells to rats to investigate the expression of APN/CD13 in primary tumors. Among the administrations, local tumor formation was induced by subcutaneous injection, and subrenal (SRCA) implantation of NeDe tumor cell line. Comparing the two different tumor models (SRCA versus subcutaneous), we found that the accumulation of both investigated radiotracers in primary tumors was higher in the SRCA model (Table 2 and 3). This difference stems from the site of the tumor cell implantation. The most commonly used method for the induction of primary tumors is the subcutaneous injection of cancer cells. This kind of transplantation is ectopic and lacking orthotopic tissue microenvironments. Vascularization and tumor growing are more intensive when tumor cells are implanted at orthotopic site (e.g. renal tumors into the kidney or subcapsular space), and the favorable microenvironment of this site may promote higher expression of angiogenic markers;

furthermore subserve tumor cell proliferation and generation of metastases (Borgstrom et al., 2013; Kerbel 2003).

By taking the SUVmean values, the uptake of ^{68}Ga-NOTA-c(NGR) of the primary tumors (subcutaneously growing NeDe tumor (Fig 3) and tumor on the left kidney (Fig 5) was relatively higher than that of the ^{68}Ga-NODAGA-[c(RGD)]$_2$ uptake, and this difference was significant ($p \leq 0.01$) in the case of SUVmax and T/M ratios at 90 min p.i.. Interestingly, Shao et al. (2014b) could not find a significant difference in T/M ratios between the applied NGR- and RGD-based probes on HT-1080 tumors. Despite that, our results suggest that ^{68}Ga-NOTA-c(NGR) bears the potential to outperform even dimeric RGD-targeted tracers, which might originate from the different structure and stability of the cyclic NGR peptide as a homing device.

After blocking by unlabeled NOTA-c(NGR), the tumor uptake of ^{68}Ga-NOTA-c(NGR) reduced significantly ($p \leq 0.01$) in both primary tumors. Similarly to previously mentioned studies with other ^{68}Ga-labeled NGR-conjugates with human xenograft tumors (Zhang et al., 2014; Shao et al., 2014a, 2014b), our successful blocking results suggest that ^{68}Ga-labeled NOTA-c(NGR) also specifically binds to the APN/CD13 receptors, which presence on NeDe tumors and metastases was proved by western blot experiments (Fig. 8).

Angiogenesis is prerequisite in the multistep process of generating metastasis when cancer cells spread from primary sites to distant places (Chaffer and Weinberg 2011). APN/CD13 may play a role in the invasion of cancer cells by enhancing their invasive capacity and metastatic behavior (Fontijn et al., 2006) and by degrading the extracellular matrix to promote malignant cell invasion (Antczak et al., 2001). Here, we used a syngenic metastasis animal model (Trencsenyi et al., 2009) to investigate the expression of APN/CD13 by ^{68}Ga-NOTA-c(NGR) not only in primary tumors, but also in metastatic lymph nodes. The implantation of NeDe tumor cells under the left kidney capsule caused tumor metastasis in the thoracal parathymic lymph nodes (PTNs) (Trencsenyi et al., 2009, 2014) and in the mesenteric lymph nodes. By *ex vivo* experiments we found APN/CD13 receptor specific accumulation of ^{68}Ga-NOTA-c(NGR) in metastatic lymph nodes (Fig. 7). These results suggest that ^{68}Ga-NOTA-c(NGR) is a promising molecular probe for the detection of metastases.

5. Conclusion

In this study, we have synthesized ^{68}Ga-NOTA-c(NGR) with high radiochemical purity and stability. Due to its high selectivity and strong binding affinity to APN/CD13, favorable biodistribution and pharmacokinetics, ^{68}Ga-NOTA-c(NGR) might be a potential molecular probe for the noninvasive detection of CD13/APN-positive tumors, metastases and neovasculature.

Conflicts of interest statement

We declare that we have no conflict of interest.

Acknowledgements

The research was supported by the Hungarian Research Fund OTKA (K 104045).
The contribution of the first author to this research project was supported by the European Union and the State of Hungary, co-financed by the European Social Fund in the framework of TÁMOP-4.2.4.A/ 2-11/1-2012-0001 ‘National Excellence Program’.

References

Antczak, C., De Meester, I., Bauvois, B., 2001. Transmembrane proteases as disease markers and targets for therapy. J. Biol. Regul. Homeostasis Agents 15, 130−139.

Arap, W., Pasqualini, R., Ruoslahti, E., 1998. Cancer treatment by targeted drug delivery to tumor vasculature in a mouse model. Science 279, 377−380.

Banerjee, S.R., Pomper, M.G., 2013. Clinical applications of Gallium-68. Appl. Radiat. Isot. 76, 2−13.

Beer, A.J., Kessler, H., Wester, H.J., Schwaiger, M., 2011. PET Imaging of Integrin αVβ3 Expression. Theranostics 17, 48−57.

Borgstrom, P., Oh, P., Czarny, M., Racine, B., Schnitzer, J.E., 2013. Co-implanting orthotopic tissue creates stroma microenvironment enhancing growth and angiogenesis of multiple tumors. Version 2. F1000Res. 2,129.

Buehler, A., van Zandvoort, M.A., Stelt, B.J., Hackeng, T.M., Schrans-Stassen, B.H., Bennaghmouch, A., Hofstra, L., Cleutjens, J.P., Duijvestijn, A., Smeets, M.B., de Kleijn, D.P., Post, M.J., de Muinck, E.D. 2006. cNGR, a novel homing sequence for CD13/APN targeted molecular imaging of murine cardiac angiogenesis in vivo. Arterioscler. Thromb. Vasc. Biol. 26, 2681−2687.

Carmeliet, P., Jain, R.K., 2000. Angiogenesis in cancer and other diseases. Nature 407, 249–257.

Chaffer, C.L., Weinberg, R.A., 2011. A Perspective on Cancer Cell Metastasis. Science 331, 1559−1564.

Chen, K., Ma, W., Li, G., Wang, J., Yang, W., Yap, L.P., Hughes, L.D., Park, R., Conti, P.S., 2013. Synthesis and evaluation of 64Cu-labeled monomeric and dimeric NGR peptides for MicroPET imaging of CD13 receptor expression. Mol. Pharm. 10, 417−427.

Colombo, G., Curnis, F., De Mori, G.M., Gasparri, A., Longoni, C., Sacchi, A., Longhi, R., Corti, A., 2002. Structure-activity relationships of linear and cyclic peptides containing the NGR tumor-homing motif. J. Biol. Chem. 27749, 47891−47897.

Corti, A., Curnis, F., Arap, W., Pasqualini, R., 2008. The neovasculature homing motif NGR, more than meets the eye. Blood 112, 2628−2635.

Corti, A., Curnis, F., 2011. Tumor Vasculature Targeting Through NGR Peptide-Based Drug Delivery Systems. Curr. Pharm. Biotechnol. 12, 1128−1134.

Corti, A., Pastorino, F., Curnis, F., Arap, W., Ponzoni, M., Pasqualini, R., 2011. Targeted drug delivery and penetration into solid tumors. Med. Res. Rev. 32, 1078−1091.

Curnis, F., Sacchi, A., Borgna, L., Magni, F., Gasparri, A., Corti, A. 2000. Enhancement of tumor necrosis factor alpha antitumor immunotherapeutic properties by targeted delivery to aminopeptidase N CD13. Nat. Biotechnol. 18, 1185−1190.

Curnis, F., Sacchi, A., Gasparri, A., Longhi, R., Bachi, A., Doglioni, C., Bordignon, C., Traversari, C., Rizzardi, G.P., Corti, A., 2008. Isoaspartate-glycine-arginine, a new tumor vasculature targeting motif. Cancer. Res. 68, 7073−7082.

Dezso, B., Rady, P., Morocz, I., Varga, E., Gomba, S., Poulsen, K., Kertai, P., 1991. Morphological and immunhistochemical characteristics of dimethylnitrosamine-induced malignant mesenchymal renal tumor in F344 rats. J. Cancer. Res. Clin. Oncol. 116, 372−378.

Dijkgraaf, I., van de Vijver, P., Dirksen, A., Hackeng, T.M., 2013. Synthesis and application of cNGR-containing imaging agents for detection of angiogenesis. Bioorg. Med. Chem. 21, 3555–3564.

Ellis, L.M., Liu, W., Ahmad, S.A., Fan, F., Jung, Y.D., Shaheen, R.M., Reinmuth, N. 2001. Overview of angiogenesis, Biologic implications for antiangiogenic therapy. Semin. Oncol. 28, 94−104.

Erdreich-Epstein, A., Tran, L.B., Cox, O.T., Huang, E.Y., Laug, W.E., Shimada, H., Millard, M., 2005. Endothelial apoptosis induced by inhibition of integrins αvβ3 and αvβ5 involves ceramide metabolic pathways. Blood 105, 4353–4361.

Faintuch, B.L., Oliveira, E.A., Targino, R.C., Moro, A.M., 2014. Radiolabeled NGR phage display peptide sequence for tumor targeting. Appl. Rad. Isot. 86, 41−45.

Fontijn, D., Duyndam, M.C.A., van Berkel, M.P.A., Yuana, Y., Shapiro, L.H., Pinedo, H.M., Broxterman, H.J., Boven, E., 2006. CD13/Aminopeptidase N overexpression by basic fibroblast growth factor mediates enhanced invasiveness of 1F6 human melanoma cells. Br. J. Cancer. 94, 1627–1636.

Folkman, J. 2002. Role of angiogenesis in tumor growth and metastasis. Semi. Oncol. 29, 15–18.

Haubner, R., 2006. αvβ3-integrin imaging, a new approach to characterise angiogenesis? Eur. J. Nucl. Med. Mol. Imaging. 33, 54−63.

Haubner, R., Wester, H.J., Burkhart, F., Senekowitsch-Schmidtke, R., Weber, W., Goodman, S.L., Kessler, H., Schwaiger, M., 2001. Glycosylated RGD-containing peptides, tracer for tumor targeting and angiogenesis imaging with improved biokinetics. J. Nucl. Med. 42, 326–336.

Haubner, R., Wester, H.J., Reuning, U., Senekowitsch-Schmidtke, R., Diefenbach, B., Kessler, H., Stöcklin, G., Schwaiger, M., 1999. Radiolabeled αvβ3 integrin antagonists, a new class of tracers for tumor targeting. J. Nucl. Med. 40, 1061–71.

van Hensbergen, Y., Broxterman, H.J., Rana, S., van Diest, P.J., Duyndam, M.C., Hoekman, K., Pinedo, H.M., Boven, E., 2004. Reduced growth, increased vascular area, and reduced response to cisplatin in CD13-overexpressing human ovarian cancer xenografts. Clin. Cancer. Res. 10, 1180−1191.

Higuchi, T., Bengel, F.M,, Seidl, S., Watzlowik, P., Kessler, H., Hegenloh, R., Reder, S., Nekolla, S.G., Wester, H.J., Schwaiger, M., 2008. Assessment of alphavbeta3 integrin expression after myocardial infarction by positron emission tomography. Cardiovasc. Res. 78, 395−403.

Kerbel, R.S., 2003. Human tumor xenografts as predictive preclinical models for anticancer drug activity in humans: better than commonly perceived-but they can be improved. Cancer Biol. Ther. 2, S134-139.

Lajtos, I., Emri, M., Kis, S.A., Opposits, G., Potari, N., Kiraly, B., Nagy, F., Tron, L., Balkay, L., 2013. Performance Evaluation and Optimization of the MiniPET-II Scanner. Nucl. Instrum. Methods. 707, 26−34.

Ma, W., Kang, F., Wang, Z., Yang, W., Li, G., Ma, X., Li, G., Chen, K., Zhang, Y., Wang, J., 2013. 99mTc-labeled monomeric and dimeric NGR peptides for SPECT imaging of CD13 receptor in tumor-bearing mice. Amino Acids 44, 1337−1345.

Ma, W., Wang, Z., Yang, W., Ma, X., Kang, F., Wang, J., 2014. Biodistribution and SPECT imaging study of 99m.Tc labeling NGR peptide in nude mice bearing human HepG2 hepatoma. BioMed Research International 2014, DOI: 10.1155/2014/618096

Negussie, A.H., Miller, J.L., Reddy, G., Drake, S.K., Wood, B.J., Dreher, M.R., 2010. Synthesis and in vitro evaluation of cyclic NGR peptide targeted thermally sensitive liposome. J. Control. Release. 143, 265–273.

Notni, J., Šimeček, J., Hermann, P., Wester, H.J., 2011. TRAP, a powerful and versatile framework for gallium-68 radiopharmaceuticals. Chem. Eur. J. 17, 14718−14722.

Pasqualini, R., Koivunen, E., Kain, R., Lahdenranta, J., et. al., 2000. Aminopeptidase N is a receptor for tumor-homing peptides and a target for inhibiting angiogenesis. Cancer. Res. 60, 722–727.

Pohle, K., Notni, J., Bussemer, J., Kessler, H., Schwaiger, M., Beer, A.J., 2012. ^{68}Ga-NODAGA-RGD is a suitable substitute for 18.F-Galacto-RGD and can be produced with high specific activity in a cGMP/GRP compliant automated process. Nucl. Med. Biol. 39, 777−784.

Rozsa, D., Trencsenyi, G., Kertai, P., Marian, T., Nagy, G., Banfalvi, G. 2009. Lymphatic spread of mesenchymal renal tumor to metastatic parathymic lymph nodes in rat. Histol. Histopathol. 24, 1367−1379.

Rundhaug, JE., 2005. Matrix metalloproteinases and angiogenesis. J. Cell. Mol. Med. 9, 267–285.

Seong Choe, Y., Lee, K.H., 2007. Targeted In Vivo Imaging of Angiogenesis, Present Status and Perspectives. Curr. Pharm. Des. 13, 17−31.

Shao, Y., Liang, W., Kang, F., Yang, W., Ma, X., Li, G., Zong, S., Chen, K., Wang, J. 2014a. ^{68}Ga-Labeled Cyclic NGR Peptide for MicroPET Imaging of CD13 Receptor Expression. Molecules 19, 11600−11612.

Shao, Y., Liang, W., Kang, F., Yang, W., Ma, X., Li, G., Zong, S., Chen, K., Wang, J., 2014b. A direct comparison of tumor angiogenesis with ^{68}Ga-labeled NGR and RGD peptides in HT-1080 tumor xenografts using microPET imaging. Amino Acids 2014 DOI: 10.1007/s00726-014-1788-x

Simons, M., 2005. Angiogenesis, Where Do We Stand Now? Circulation 111, 1556−1566.

Smith, D.L., Breeman, W.A., Sims-Mourtada , J., 2013. The untapped potential of Gallium 68-PET, the next wave of ^{68}Ga-agents. Appl. Radiat. Isot. 76, 14−23.

Su, L., Cao, J., Jia, Y., Zhang, X., Fang, H., Xu, W., 2012. Development of Synthetic Aminopeptidase N/CD13 Inhibitors to Overcome Cancer Metastasis and Angiogenesis. ACS Med. Chem. Lett. 3, 959−964.

Trencsenyi, G., Kertai, P., Bako, F., Hunyadi, J., Marian, T., Hargitai, Z., Pocsi, I., Muranyi, E., Hornyak, L., Banfalvi, G. 2009. Renal capsule-parathymic lymph node complex, a new in vivo metastatic model in rats. Anticancer. Res. 29, 2121−2126.

Trencsenyi, G., Nagy, G., Kahlik, B., Nemeth, E., Kertai, P., Kiss, A., Banfalvi, G., 2014. Lymphoid metastasis of rat My2/De leukemia. Leuk. Res. 5, 586−593.

Velikyan, I., 2013. Prospective of ^{68}Ga-radiopharmaceutical development. Theranostics 4, 47–80.

Wang, R.E., Niu, Y., Wu, H., Amin, M.N., Cai, J., 2011. Development of NGR peptide-based agents for tumor imaging. Am. J. Nucl. Med. Mol. Imaging. 1, 36–46.

Wängler, C., Wängler, B., Lehner, S., Elsner, A., Todica, A., Bartenstein, P., Hacker, M., Schirrmacher, R., 2011. A universally applicable ^{68}Ga-labeling technique for proteins. J. Nucl. Med. 52, 586−591.

Wester, H.J., 2007. Nuclear imaging probes, from bench to bedside. Clin. Cancer. Res. 13, 3470−3481.

Workman, P., Twentyman, P., Balkwill F, et al., 1988. United Kingdom Coordinating Committee on Cancer Research UKCCCR. Guidelines for the welfare of animals in experimental neoplasia. Br. J. Cancer. 77, 1−10.

Wu, C., Li, F., Niu, G., Chen, X. 2013. PET imaging of inflammation biomarkers. Theranostics 3, 448−466.

Yancopoulos, G.D., Davis, S., Gale, N.W., Rudge, J.S., Wiegand, S.J., Holash, J., 2000. Vascular-specific growth factors and blood vessel formation. Nature 407, 242−248.

Yang, Y., Yang, Y., Xie, X., Cai, X., Zhang, H., Gong, W., Wang, Z., Mei, X., 2014. PEGylated liposomes with NGR ligand and heat-activable cell-penetrating petide-doxorubicin conjugate for tumor-specific therapy. Biomaterials 35, 4368−4381.

Zhang, J., Lu, X., Wan, N., Hua, Z., Wang, Z., Huang, H., Yang, M., Wang, F., 2014. ^{68}Ga-DOTA-NGR as a novel molecular probe for APN-positive tumor imaging using MicroPET. Nucl. Med. Biol. 41, 268−275.